Modulation instability in higher-order nonlinear Schrödinger equations

Amdad Chowdury,[1] Adrian Ankiewicz,[2] Nail Akhmediev,[2] and Wonkeun Chang[1,a)]
[1]*School of Electrical and Electronic Engineering, Nanyang Technological University, Singapore 639798*
[2]*Optical Sciences Group, Research School of Physics and Engineering, The Australian National University, Canberra, Australian Capital Territory 2600, Australia*

(Received 28 August 2018; accepted 19 November 2018; published online 17 December 2018)

We investigate the dynamics of modulation instability (MI) and the corresponding breather solutions to the extended nonlinear Schrödinger equation that describes the full scale growth-decay cycle of MI. As an example, we study modulation instability in connection with the fourth-order equation in detail. The higher-order equations have free parameters that can be used to control the growth-decay cycle of the MI; that is, the growth rate curves, the time of evolution, the maximal amplitude, and the spectral content of the Akhmediev Breather strongly depend on these coefficients. *Published by AIP Publishing.* https://doi.org/10.1063/1.5053941

The nonlinear Schrödinger equation (NLSE) is used widely for modeling nonlinear wave propagation in dispersive media. Although this equation is the simplest member of a family of integrable equations, it has a variety of analytic solutions in the form of solitons, breathers, and rogue waves. In particular, the Peregrine solution describes the appearance of giant waves in deep oceans, as well as the formation of extremely high amplitude pulses in optical fibers. On the other hand, the family of breather solutions describes the phenomenon that is called modulation instability (MI).

The accuracy provided by the NLSE is sufficient for a description of the main features of these phenomena. Nevertheless, we should remember the limitations that materialize when only the lowest-order dispersion and nonlinear terms are used. The higher-order dispersion and nonlinear terms should be taken into account to improve the accuracy of the equation. However, the higher-order terms cannot simply be added in a haphazard fashion, as this may destroy the integrability that is extremely helpful for obtaining analytic solutions. In this work, we study the MI dynamics in the case when the higher-order terms preserve the integrability of the extended NLSE.

I. INTRODUCTION

Modulation instability (MI) is one of the key processes that initiates the formation of periodic structures in nonlinear dispersive media. This is a mechanism where a background carrier wave is modulated due to seeding periodic perturbations that initially grow but may also decay. New frequencies are generated during this process and intensive energy exchange occurs between them. MI can produce an unlimited number of new frequency components, resulting in periodic trains of localized waves or pulses.[1] This effect has widespread manifestations in natural phenomena and applications in technology.

MI has been studied in optics,[2] hydrodynamics,[3,4] plasmas,[5] and biology[6]. In nonlinear optics, MI has been the subject of extensive study because of its inherent connection with short pulse train generation in nonlinear optical media,[7] as well as optical parametric amplification.[8,9] The underlying mechanism involved in the initial stage of supercontinuum generation is closely connected to noise-driven MI.[10–12] It has been revealed that the emergence of an optical rogue wave in the supercontinuum generation process is connected to MI.[12,13] The well-known Fermi-Pasta-Ulam (FPU-T) recurrence phenomenon, that has been studied in Ref. 14, is also closely related to MI.[15–18]

The propagation of ultra-short optical pulses in nonlinear dispersive media is often modeled using the nonlinear Schrödinger equation (NLSE) in its various forms.[19] Indeed, the integrable form of the NLSE[20] has the advantage of having analytic solutions that include solitons. The exact solution that describes the full scale growth-decay cycle of MI is known as the Akhmediev Breather (AB).[21,22] A large amount of literature is available on the use of ABs in physics.[12,15,23–30]

In the context of nonlinear optics, the basic NLSE, which only includes the lowest-order dispersive and nonlinear terms, can accurately model relatively long optical pulses.[31] As the pulse durations become shorter, other nonlinear effects, such as self-steepening and Raman effect, become important.[19] Then, the basic NLSE needs to be improved by including higher-order terms that are related to these effects. MI in this so-called generalized NLSE has been subject to numerous investigations in the field of ultrafast optics, as it closely models the noise-induced supercontinuum generation process.[10,32]

The NLSE can also approximate the dynamics of ocean surface gravity waves.[33,34] A comparative study of waves in optical fibers and on water surfaces reveals a common phenomenon such as supercontinuum generation.[35] The NLSE approximation has been improved by Dysthe, taking into account the two-dimensional nature of the ocean surface.[36] Even in the case of unidirectional wave propagation, correction terms are still necessary to obtain higher accuracy in the wave modeling.[37,38] The general structure of these correction terms is the same as for those relating to optical fibers, as they are higher-order terms for the dispersion and nonlinear response of the medium. However, the coefficients defining the values of these corrections differ.

a)Electronic mail: wonkeun.chang@ntu.edu.sg

Arbitrary coefficients result in a non-integrable equation which make the general analysis difficult. Then, the only way to obtain detailed results is to carry out numerical simulations for each particular choice of the coefficients. On the other hand, some specific choices of the coefficients provide integrability, and then the results can be expressed in analytic forms.[39–43]

One of the phenomena related to the NLSE is modulation instability (MI). In the water wave case, it is known as the Benjamin-Feir instability.[44,45] The modification of the NLSE also changes the instability curves for the range of wavelengths covered by the instability.[46] Importantly, MI has been recognized as one of the sources for the appearance of rogue waves in the ocean.[47] As MI represents only the initial stage of long-term evolution, the detailed analysis of both the MI stage and the follow-up growth-decay dynamics (AB) are equally important for a complete analysis.

The aim of the present work is to provide analytic results for MI and AB stages of unidirectional wave evolution for the extended NLSE, where the coefficients of the higher-order terms are chosen to make the whole equation integrable. This choice may not provide a direct answer to practical problems, but it is closer than the basic NLSE to realistic situations. Indeed, we find that the AB solutions, and the corresponding properties of MI, differ from the NLSE case. Moreover, our analysis allows us to take into account an infinite number of correction terms. The latter was not possible in any of the previous approaches. As we shall see, the MI growth rate changes significantly with increasing equation order. The higher-order terms have a large impact, both on the MI characteristics and the AB stage of wave evolution.

II. HIGHER-ORDER NLS EQUATIONS AND THEIR BREATHER SOLUTIONS

We start with the extended integrable NLS equation with an infinite number of free parameters[39,42]

$$\begin{aligned} &i\psi_x + \alpha_2 S_2[\psi(x,t)] - i\alpha_3 S_3[\psi(x,t)] \\ &\quad + \alpha_4 S_4[\psi(x,t)] - i\alpha_5 S_5[\psi(x,t)] + \cdots = 0, \end{aligned} \tag{1}$$

where the complex-valued function $\psi(x,t)$ represents the envelope of the waves, x is the variable along the propagation direction, and t is the time variable in a frame moving with the group velocity of waves. Equation (1) is written in the operator form with each $S_j[\psi(x,t)]$ $(j = 2,3,\ldots)$ representing the jth order functional. In particular, $S_2[\psi(x,t)]$ is the standard nonlinear Schrödinger operator.[1] It includes second-order dispersion and Kerr-type nonlinearity

$$S_2[\psi(x,t)] = \psi_{tt} + 2\psi|\psi|^2. \tag{2}$$

If all coefficients α_j are zero except for α_2 then Eq. (1) is the basic NLSE. For the third order case, we have $S_3[\psi(x,t)]$ as the Hirota operator[48,49]

$$S_3[\psi(x,t)] = \psi_{ttt} + 6|\psi|^2\psi_t. \tag{3}$$

When only two coefficients α_2 and α_3 are nonzero, Eq. (1) is the so-called Hirota equation. The fourth-order functional, $S_4[\psi(x,t)]$, is the Lakshmanan-Porsezian-Daniel (LPD) operator[50–52]

$$\begin{aligned} S_4[\psi(x,t)] = {} & \psi_{tttt} + 8|\psi|^2\psi_{tt} + 6\psi|\psi|^4 \\ & + 4\psi|\psi_t|^2 + 6\psi_t^2\psi^* + 2\psi^2\psi_{tt}^*. \end{aligned} \tag{4}$$

Porsezian *et al.*[53] derived this equation in connection with integrability aspects of a one-dimensional Heisenberg spin chain problem. The next, fifth-order operator, $S_5[\psi(x,t)]$, is given by Refs. 41 and 54:

$$\begin{aligned} S_5[\psi(x,t)] = {} & \psi_{ttttt} + 10|\psi|^2\psi_{ttt} + 30|\psi|^4\psi_t \\ & + 10\psi\psi_t\psi_{tt}^* + 10\psi\psi_t^*\psi_{tt} \\ & + 20\psi^*\psi_t\psi_{tt} + 10\psi_t^2\psi_t^*. \end{aligned} \tag{5}$$

A method for deriving this infinite number of higher-order operators is given in Ref. 42. Three of them, viz. $S_6[\psi(x,t)]$, $S_7[\psi(x,t)]$, and $S_8[\psi(x,t)]$, are given explicitly in Appendix A of Ref. 42. We stress that Eq. (1), with an infinite number of free parameters, α_j, is integrable and that its solutions can be written in the analytical form. Importantly, the odd and even order operators introduce different features to the solutions. For example, odd order operators (3) and (5) introduce *velocity* or *rotation* in the x,t-plane to the solutions[43,55] while the even order operators (2) and (4) do not. Instead, they change the MI characteristics and influence the *phase* of the solutions.[40,42,56,57]

In the present work, we provide a comprehensive description of how higher-order terms in Eq. (1) affect the AB dynamics. We consider only the even order terms, as only they are known to change the features of MI. To start with, we give the general first-order AB solution to Eq. (1) derived for the case of an infinite number of even order terms

$$\psi_1 = \left(\frac{\kappa\{\kappa\cosh[V_H x_s] + iv_1\sinh[V_H x_s]\}}{2\cosh[V_H x_s] - v_1\cos[\kappa t_s]} - 1 \right) e^{i\omega x}, \tag{6}$$

where $V_H = \Omega\delta$ and $\delta = \frac{1}{2}\kappa\sqrt{4-\kappa^2}$ with $0 < \kappa < 2$, $v_1 = \sqrt{4-\kappa^2}$ and $x_s = x - x_0$ and $t_s = t - t_0$. The parameters x_0 and t_0 are translations along x and t axes. κ is the modulation frequency of the breather and V_H is the growth rate of the modulation at $x \to -\infty$. The parameter Ω is given by

$$\begin{aligned} \Omega &= 2\sum_{n=0}^{N} \alpha_{2n+2} \frac{(2n+1)!}{(n!)^2} {}_2F_1\left(1, -n; \frac{3}{2}; \frac{\kappa^2}{4}\right) \\ &= 2\left[\alpha_2 + \alpha_4\left(6-\kappa^2\right) + \alpha_6\left(30 - 10\kappa^2 + \kappa^4\right) + \cdots\right], \end{aligned} \tag{7}$$

where ${}_2F_1$ is a hypergeometric function. The propagation constant (or phase factor) ω is

$$\omega = \sum_{m=1}^{M} \alpha_{2m} \frac{(2m)!}{(m!)^2} = 2(\alpha_2 + 3\alpha_4 + 10\alpha_6 + \cdots). \tag{8}$$

For an infinite number of even order operators, $N = M = \infty$. This solution has been presented earlier in Refs. 40, 42, 56, and 57. It has the same form as the AB for the NLSE case[21,22] except for more complicated expressions for the coefficients.

In Secs. III, IV, and V, we mainly restrict ourselves to the two even-order operators S_2 and S_4 in Eq. (1). That is, we are

dealing with the equation

$$i\psi_x + \alpha_2(\psi_{tt} + 2\psi|\psi|^2) + \alpha_4(\psi_{tttt} + 8|\psi|^2\psi_{tt} + 4\psi|\psi_t|^2 + 6\psi_t^2\psi^* + 2\psi^2\psi_{tt}^* + 6\psi|\psi|^4) = 0 \quad (9)$$

that has been considered earlier in Refs. 58 and 59. The coefficient α_2 in Eq. (9) scales the terms of the standard NLSE while the coefficient α_4 scales the fourth-order terms. Without loss of generality, the coefficient α_2 can be fixed to $\alpha_2 = \frac{1}{2}$. In Sec. III, we take Eq. (9) as a representative example of the equation with even-order operators and discuss the basic features of the MI growth rate for both positive and negative signs of α_4. In Sec. IV, we discuss the properties of AB in the frequency domain. In Sec. V, we consider the AB trajectories on a complex plane. In Sec. VI, we discuss the total AB phase shift. Finally, in Sec. VII, we give a brief description of MI for the equation with 6th and 8th order terms. We show that higher-order even operators exhibit similar MI properties, except that they have different zero points within the instability band. Our analysis can be easily extended to equations with any number of even order terms, as the exact solution (6) is valid for all of them.

III. GROWTH RATE OF INSTABILITY

We start by analyzing fundamental breather solutions and their particular cases. If we take the summation up to $N = 0$ in Eq. (7) and $M = 1$ in Eq. (8), we obtain the first-order AB solution of the NLSE. In other words, the breather solution of Eq. (9) with $\alpha_2 = 1/2$ and $\alpha_4 = 0$ is given by

$$\psi_1 = \left(\frac{\kappa\{\kappa\cosh[\delta x_s] + iv_1\sinh[\delta x_s]\}}{2\cosh[\delta x_s] - v_1\cos[\kappa t_s]} - 1\right)e^{ix}. \quad (10)$$

For this case, we have $\Omega = \omega = 1$ and the growth rate $V_H = \delta$ in Eq. (6). The periodic perturbations on a finite background will grow only when κ remains within the modulation instability band $0 < \kappa < 2$. This condition makes the growth rate δ real. This solution was first presented in the explicit form in Refs. 21 and 22. The solution is periodic in t and localized in x within one full growth-decay cycle. A detailed description of this solution, its connection to FPU-T recurrence phenomena, and its frequency spectrum analysis have been presented in Refs. 1, 16, and 60.

Now, if we go one step beyond the NLSE, and take into account the next higher-order even term, we obtain Eq. (9). The additional terms in Eq. (9) take into account higher-order dispersion and higher-order nonlinear terms that have to be considered when accurately modeling ultra-short pulse propagation in optical fibers. These terms inevitably modify the features of the MI phenomenon. The best way to describe these changes is to analyze the exact solution. If we raise the summation to $N = 1$ in Eq. (7) and $M = 2$ in Eq. (8), we obtain the first-order AB solution of Eq. (9). The solution has the same form as Eq. (6) but the growth rate is now given by

$$V_H = 2\delta[\alpha_2 - \alpha_4(\kappa^2 - 6)] \quad (11)$$

and the propagation constant is given by $\omega = 2(\alpha_2 + 3\alpha_4)$. We can see, from Eq. (11), that the modified growth rate V_H depends on free parameters α_2 and α_4. It is shown in Fig. 1 for several values of α_4 and fixed $\alpha_2 = 1/2$. For comparison, the

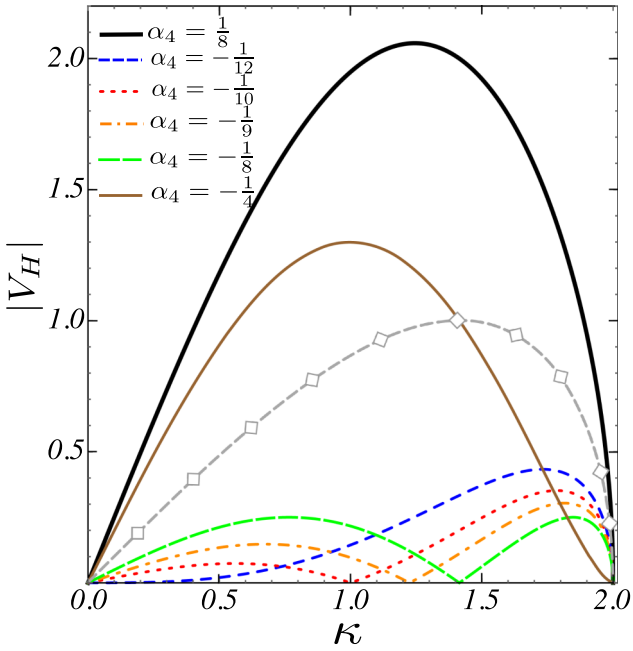

FIG. 1. The growth rate of modulation $|V_H|$ versus frequency κ for Eq. (9) for various values of α_4. The uppermost *black-thick curve* is for $\alpha_4 = 1/8$. It is located above the growth rate for the NLSE case ($\alpha_4 = 0$) presented by the *gray-dashed curve* marked with blank diamonds. The growth rates for negative α_4 values, $-1/10$; $-1/9$; and $-1/8$, are shown as *red-dotted*, *orange dot-dashed*, and *green long-dashed* curves, respectively. They become zero at $\kappa = 1$, $\sqrt{\frac{3}{2}}$, and $\sqrt{2}$. For $\alpha_4 = -1/12$ and $-1/4$, shown as *blue-dashed* and *brown-thin solid* curves, the MI curve is positive in the whole interval of κ values within 0 and 2.

NLSE case, $\alpha_4 = 0$, is also shown and is depicted by the gray dashed curve. We are dealing with the focusing case $\alpha_2 > 0$ and this leaves us with two possibilities: (a) $\alpha_4 > 0$ and (b) $\alpha_4 < 0$.

Any positive value of α_4 simply increases the growth rate. As can be seen from Fig. 1, the whole black-thick curve, calculated for $\alpha_4 = 1/8$, is located above the growth rate curve for the NLSE case. This, in effect, leads to faster evolution of a breather with a higher growth rate. However, when α_4 is negative, the growth rate can be reduced and may reach zero at some frequency within the instability band. In the latter case, the gain curve may have two local maxima, as Fig. 1 shows. The condition of zero growth rate, $V_H = 0$, leads to an algebraic equation relative to the frequency κ:

$$1 - 2(\kappa^2 - 6)\alpha_4 = 0. \quad (12)$$

The solution within the instability band $0 < |\kappa| < 2$ is $\kappa = \kappa_s = \sqrt{(6 + \frac{1}{2\alpha_4})}$. This restricts the allowable values for α_4 to the interval $-\frac{1}{4} < \alpha_4 < -\frac{1}{12}$. At the left-hand-side ($\alpha_4 = -\frac{1}{4}$) of this interval, $\kappa_s \to 2$, while at the right-hand-side ($\alpha_4 = -\frac{1}{12}$), $\kappa_s \to 0$ (see Fig. 6).

Within this interval of α_4 and for $\alpha_2 = 1/2$, the growth rate V_H becomes zero at three points, $\kappa = 0$, κ_s, and 2. For the particular cases shown in Fig. 1, we have the following numbers:

- For $\alpha_4 = -1/10$, the *red-dotted* curve hits the horizontal axis at $\kappa_s = 1$. The two growth rate maxima of the resulting instability sub-bands are located at $\kappa = \frac{1}{2}\sqrt{7 \pm \sqrt{33}}$.
- For $\alpha_4 = -1/8$ (*green dashed* curve), $\kappa_s = \sqrt{2}$. The maximum gain occurs at two points, $\kappa = \sqrt{2 \pm \sqrt{2}}$. The two gain maxima in this case are of equal values.
- For $\alpha_4 = -1/9$ (*orange dot-dashed* curve), $\kappa_s = \sqrt{\frac{3}{2}}$. The maximal growth rates in the two sub-bands occur at the points $\kappa = \frac{1}{2}\sqrt{\frac{1}{2}(15 \pm \sqrt{129})}$.

When the growth rate is zero at $\kappa = \kappa_s$, Eq. (6) turns into a propagation-invariant solution periodic in t:

$$\psi_1 = \left(\frac{\kappa_s^2}{2 - \sqrt{4 - \kappa^2}\cos[\kappa_s t_{s1}]} - 1 \right) e^{i\omega' x}, \tag{13}$$

where the propagation constant $\omega' = 2\alpha_4(\kappa_s^2 - 3)$. Solution (13) has been presented earlier in Ref. 57 [see Eq. (3)].

For the NLSE case, the growth rate is maximal ($\delta = 1$) at the point $\kappa = \sqrt{2}$. The peak amplitude of the AB is the highest at this point. Above this point, the growth rate and the peak amplitude reduce up to $\kappa = 2$, where the AB reduces to the background plane wave.

On the other hand, for the fourth-order equation with negative α_4, the instability band is split into two sub-bands at the point $\kappa = \kappa_s$. The two sub-bands generally have two distinct gain maxima with the maximum on the left-hand-side being lower than the maximum on the right-hand-side, apart from the case $\alpha_4 = -1/8$, when they are equal. A non-zero growth rate defines the longitudinal length of the breather. The breather is transformed into a propagation invariant periodic solution (13) at $\kappa = \kappa_s$. The breather is transformed into a plane wave at $\kappa = 2$. At the limits of α_4, i.e., when $\alpha_4 = -1/4$ and $-1/12$, we get a single instability band, just as in the NLSE case. However, the shape of the growth rate curve is different from the curve for the NLSE case.

IV. EVOLUTION OF THE AB SPECTRA

Spectral evolution of the AB for the NLSE case has been studied in Refs. 1, 16, and 60. The exact solution (6) allows us to find the spectral modes for the equation with infinitely many even-order operators. That is, the nth spectral component, which has frequency $n\kappa$, i.e., the nth harmonic of the MI frequency is

$$f_n(x) = \frac{\kappa}{2\pi} e^{ix\omega} \int_0^{2\pi/\kappa} \psi_1 \cos(n\kappa t) dt \tag{14}$$

$$= \frac{\kappa}{2\pi} e^{ix\omega} \int_0^{2\pi/\kappa} \left[\frac{p(x)}{2\cosh(V_H x) - v_1 \cos(\kappa t)} - 1 \right] \times \cos(n\kappa t) dt. \tag{15}$$

This general expression is valid for any number of terms in the evolution Eq. (1). Below, we consider only the case with non-zero α_2 and α_4. We then have

$$\begin{pmatrix} p(x) = \kappa\left\{\kappa\cosh[V_H x] + iv_1 \sinh[V_H x]\right\} \\ V_H = \kappa\sqrt{4 - \kappa^2}\left[\alpha_2 - \alpha_4\left(\kappa^2 - 6\right)\right] \end{pmatrix}.$$

First, we take $\kappa = \sqrt{2}$. This value simplifies the expressions for the power spectrum, while allowing us to study the evolution of the spectral content without losing generality. In this case

$$|f_0(x)|^2 = 3 - 2\sqrt{2}\cosh(2Bx)\sqrt{\operatorname{sech}(4Bx)},$$

$$|f_1(x)|^2 = 2\Big\{1 + 2\cosh(4Bx) - \sqrt{2}\big[\cosh(2Bx) + \cosh(6Bx)\big]\sqrt{\operatorname{sech}(4Bx)}\Big\},$$

$$|f_2(x)|^2 = \frac{1}{g}\sqrt{2}\Big\{\sqrt{2}g[5 + 8\cosh(4Bx)] + 4\sqrt{2}g\cosh(8Bx) - 4[2 + 2\sqrt{2}\cosh(2Bx) + \cosh(4Bx)][2\cosh(2Bx) + \cosh(6Bx)] \times \frac{1}{\sqrt{\cosh(4Bx)}}\Big[1 + \cosh(4Bx) + 2\sqrt{\cosh(4Bx)}\sqrt{\operatorname{sech}(4Bx)}\sinh^2(2Bx)\Big]\Big\},$$

where

$$g(x) = 2 + 2\sqrt{2}\cosh(2Bx) + \cosh(4Bx),$$
$$B = \alpha_2 + 4\alpha_4.$$

There is no problem in writing down similar expressions for any κ within the interval between 0 and 2. The MI growth rate in this case can be controlled by the value of α_4. If the growth rate is close to zero, the evolution takes a much longer propagation distance than it does when the gain is higher. Let us illustrate this by particular examples. The spectral evolution for two cases, (a) $\alpha_4 = -10/79 \approx -1/8$ and (b) $\alpha_4 = 1/12$, are shown in Figs. 2(a) and 2(b), respectively. In the first case $|V_H|$ is close to zero. Thus, the MI evolution takes longer than in the case (b), where $|V_H|$ is much larger.

In each case, the power is mostly concentrated in the lower order harmonics ($n = 0, 1$, and 2). The black dotted curve represents the sum of the power in the pump and two lowest order sidebands. The highest amplitude of the sidebands is reached at $x = 0$

$$|f_n(0)|^2 = 2(\sqrt{2} - 1)^{2|n|}, |n| \geq 1,$$

while the power in the fundamental mode is

$$|f_0(0)|^2 = (\sqrt{2} - 1)^2.$$

As the left and right hand sidebands contain equal power, $|f_{-n}| = |f_n|$, the total power is given by

$$|f_0(0)|^2 + 2\sum_{n=1}^{\infty} |f_n(0)|^2 = 1.$$

We also note that

$$\log\left[|f_n(0)|^2\right] = 4|n|\ \log(\sqrt{2} - 1)\ \approx\ 0.693 - 1.763|n|,$$

confirming that the triangular shape of the AB spectrum is retained for this case. When $\alpha_2 = 1/2$, a positive α_4 simply reinforces the focusing effect and increases the growth rate, resulting in a faster breather evolution at any κ. We now look at how the spectral evolution differs in the two instability

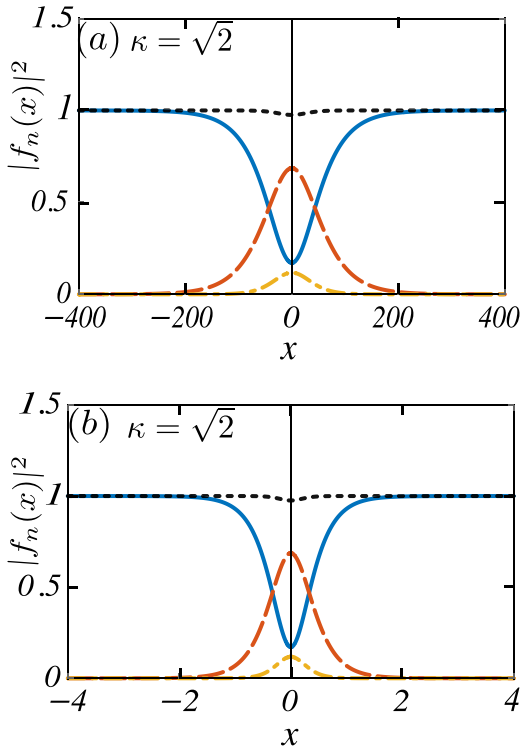

FIG. 2. Plot of the AB spectra $|f_n(x)|^2$ versus x when (a) $\alpha_4 = -10/79$ and (b) $\alpha_4 = 1/12$. In each case $\kappa = \sqrt{2}$ and $\alpha_2 = 1/2$. The pump power, $|f_0(x)|^2$, is shown in the blue solid line; the power in the first sideband, $|f_1(x)|^2$, is plotted in the dark orange dashed line, and the power in the second sideband, $|f_2(x)|^2$, is shown in the yellow dot-dashed line. The black dotted curve is the sum of the power in the pump and the two lowest sidebands, $|f_0(x)|^2 + 2|f_1(x)|^2 + 2|f_2(x)|^2$. The growth-return cycle in (a) occurs over a much larger distance in x than in (b).

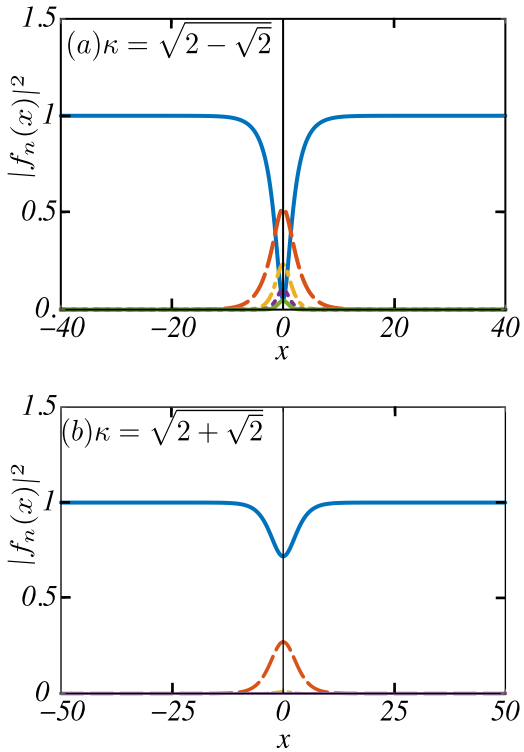

FIG. 3. The spectral evolution of AB for $\alpha_4 = -1/8$ when (a) $\kappa = \sqrt{2-\sqrt{2}}$ and (b) $\kappa = \sqrt{2+\sqrt{2}}$. These κ values correspond to the two gain maxima shown in Fig. 1. The central component $|f_0(x)|^2$ is shown by the blue solid curve. The other components, $|f_n(x)|^2$ are for $n = \pm1, \pm2, \pm3$, and ±4. Their amplitudes are smaller in (b). In all cases, $\alpha_2 = 1/2$.

sub-bands when α_4 is negative. We consider the most representative example of $\alpha_4 = -1/8$, when the two gain maxima at $\kappa = \sqrt{2-\sqrt{2}}$ and $\kappa = \sqrt{2+\sqrt{2}}$ are equal. The forms of spectral evolution at these two κ values are shown in Figs. 3(a) and 3(b), respectively. The two plots are considerably different. At the first maximum, $\kappa = \sqrt{2-\sqrt{2}}$, the power at the pump frequency $f_0(x)$ (blue solid curve) is depleted almost entirely at $x = 0$. Correspondingly, the power in the sidebands is higher. In contrast, the pump only partly depletes at the second gain maximum, $\kappa = \sqrt{2+\sqrt{2}}$. Most of the power is converted into the first sideband, as can be seen from Fig. 3(b). The power in the other sidebands is very small.

At the zero instability point, $\kappa = \kappa_s$, the solution is periodic in t but does not vary in x. The spectral content of this solution is fixed. Figure 4 shows the central and sideband power composition at this point for a varying α_4. The change of κ_s with α_4 is also shown on this plot by the blue curve with red circles. Interestingly, the power in the central component is zero when $\alpha_4 = -1/10$ and $\kappa_s = 1$. This means that the sidebands have the largest power. This value could be optimal for breathers at modulation frequencies near this κ_s. At $\alpha_4 = -1/4$, the solution is transformed into a plane wave. Consequently, all the energy is in the central component. The solution is not defined for the upper limit at $\alpha_4 = -1/12$. This point is indicated with a black dashed vertical line in Fig. 4.

V. AB EVOLUTION TRAJECTORIES IN THE COMPLEX PLANE

The evolution of the breathers can be illustrated as trajectories in the complex plane if we follow the evolution of their points of maximal (minimal) amplitude. These curves are projections of trajectories of an infinite-dimensional dynamical system in a full phase space onto a plane. These trajectories are shown in Fig. 5(a). They show the motion of the point $\psi(x, t = 0)$ with x for fixed α_4 and κ. Trajectories start at one of the points on a unit circle that corresponds to the background plane wave with an arbitrary initial phase. Any

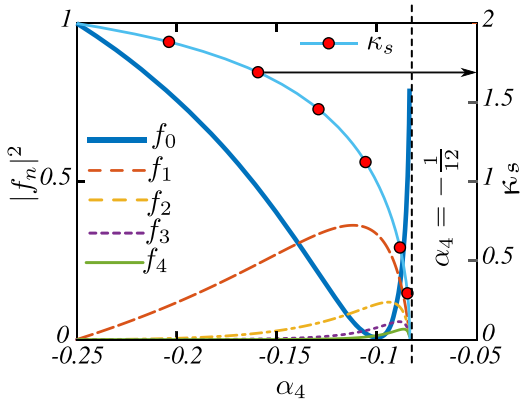

FIG. 4. The spectral power $|f_n|^2$ for $n = 0, 1, 2, 3, 4$ versus α_4 when $\kappa = \kappa_s$. The curves are obtained using Eqs. (14) and (15). As the spectrum is x invariant in this case, $f_n(x) = f_n$.

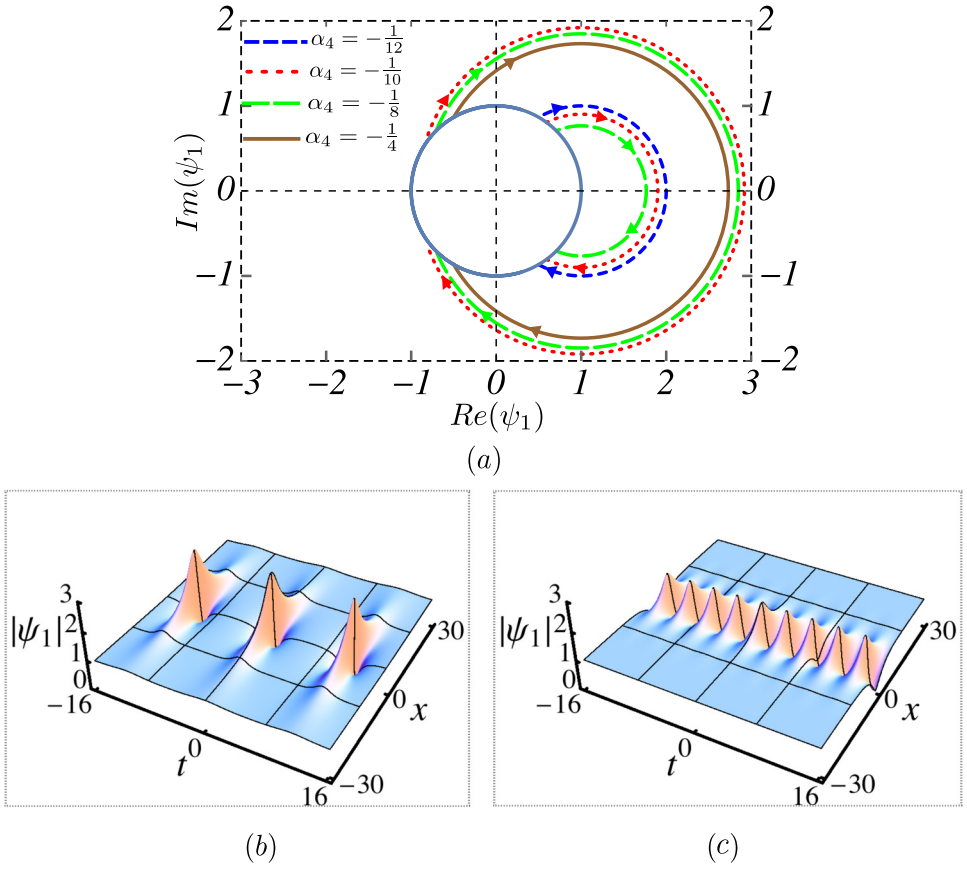

FIG. 5. (a) AB trajectories on the complex plane for the values of $\alpha_4 = -\frac{1}{12}, -\frac{1}{10}, -\frac{1}{8}$, and $-\frac{1}{4}$. Color coding of the curves is shown in the inset. The *solid light blue curve* is the unit-circle of initial conditions, which represents the background wave. (b) The AB solution for $\kappa = \frac{1}{2}\sqrt{7-\sqrt{33}}$ corresponds to the outer *red-dotted* trajectory in (a). (c) The AB solution for $\kappa = \frac{1}{2}\sqrt{7+\sqrt{33}}$ corresponds to the inner *red-dotted* trajectory in (a). For both cases (b) and (c), the parameters are $\alpha_4 = -1/10$ and $\alpha_2 = 1/2$.

point on this circle is a saddle point that corresponds to MI. The point $\psi(x, t = 0)$ moves away from the circle, returning to the circle of initial conditions after crossing the real axis at the point of maximum amplitude. The direction of motion is shown by the arrows on the trajectories in Fig. 5(a). The exact solution shows that these trajectories are also circles.

The two *red-dotted* trajectories in Fig. 5(a) are shown for the case $\alpha_4 = -1/10$. They correspond to the two MI growth rate maxima in Fig. 1 at $\kappa = \frac{1}{2}\sqrt{7-\sqrt{33}}$ (outer trajectory) and $\kappa = \frac{1}{2}\sqrt{7+\sqrt{33}}$ (inner trajectory). Although the gain is higher at the second maximum, resulting in faster evolution, the solution reaches a higher peak amplitude at the first maximum. This can be seen from Figs. 5(b) and 5(c), which show the ABs at these two points. The maximal amplitudes of the two ABs are given by the expression $\psi(0,0) = \frac{1}{2}\left(2+\sqrt{9\pm\sqrt{33}}\right)$.

The two *green-dashed* trajectories in Fig. 5(a) are shown for the case $\alpha_4 = -1/8$. The two maxima of the MI growth rate in Fig. 1 are located at the points $\kappa = \sqrt{2-\sqrt{2}}$ and $\kappa = \sqrt{2+\sqrt{2}}$. Even though the growth rates are equal at these maxima, the solutions evolve differently. The breather at the first maximum achieves a higher amplitude at $x = 0$ than at the second maximum.

Only one trajectory (*blue small-dashed* curve) is shown for the case $\alpha_4 = -1/12$. In this case, there is a single maximum of the growth rate at $\kappa = \sqrt{3}$. Finally, the *brown solid* curve corresponds to $\alpha_4 = -1/4$. Here, we also have a single maximum of the growth rate curve at $\kappa = 1$. The trajectory of the periodic solution (13) is simply a dot located on the real axis, no matter what value is taken by κ_s. However, its position does depend on κ_s.

VI. NONLINEAR PHASE SHIFT INDUCED BY THE AB

Every breather induces a phase shift that is the difference between the phase in the presence of, and in the absence of, the breather on top of a background wave.[16,18] It is defined as a phase rotation from the initial to the final point of the trajectory on the complex plane. This phase shift explicitly depends on κ, and it can be calculated from Eq. (14):

$$\Delta\phi = 2\cos^{-1}\left[\frac{1}{2}\left(\kappa^2 - 2\right)\right], \quad \text{for all}\, \kappa \neq \kappa_s. \tag{16}$$

This phase shift is same as for the AB in the NLSE case. However, when $\kappa = \kappa_s$ for a given α_4, the solution remains fixed along the x-axis and the total phase shift is zero.

VII. THE INFLUENCE OF THE 6TH AND 8TH ORDER TERMS

In order to determine the role of operators above 4th order, we next consider the 6th and 8th order terms in the evolution Eq. (1). Our main conclusion is that the influence of the higher-order even operators, e.g., 6th and 8th order operators with non-zero α_2 coefficient is qualitatively similar to that of the 4th order term. For a more detailed analysis, we set $\alpha_4 = 0$ and study the MI in this case. The AB solution is still

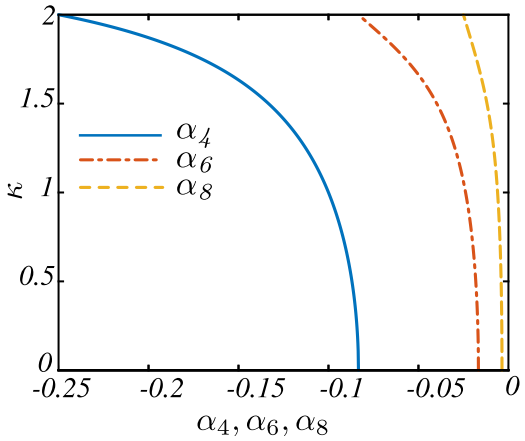

FIG. 6. Modulation frequency that leads to the zero growth rate versus the higher-order operator coefficient α_4, α_6, or α_8 in the evolution equation.

the same and is given by Eq. (6). With $N = 2$ and 3 in Eq. (7) and $M = 3$ and 4 in Eq. (8), the instability growth rates are now given by higher-order polynomials:

$$V_H^{(6)} = 2\delta[\alpha_2 - \alpha_6(10\kappa^2 - \kappa^4 - 30)], \tag{17}$$

$$V_H^{(8)} = 2\delta[\alpha_2 - \alpha_8(70\kappa^2 - 14\kappa^4 + \kappa^6 - 140)]. \tag{18}$$

The propagation constants now are

$$\omega^{(6)} = 2(\alpha_2 + 10\alpha_6),$$
$$\omega^{(8)} = 2(\alpha_2 + 35\alpha_8).$$

At the points of zero growth rate, $V_H^{(6)} = 0$ and $V_H^{(8)} = 0$, the AB solution reduces to the constant profile periodic solution of (13). The propagation constants in this case are

$$\omega'^{(6)} = -2(20 - 10\kappa^2 + \kappa^4),$$
$$\omega'^{(8)} = 2(-105 + 70\kappa^2 - 14\kappa^4 + \kappa^6).$$

The points of zero MI growth rate can be found from algebraic equations. Keeping the fixed value of $\alpha_2 = 1/2$, we have

$$1 - 2(10\kappa^2 - \kappa^4 - 30)\alpha_6 = 0, \tag{19}$$

$$1 - 2(70\kappa^2 - 14\kappa^4 + \kappa^6 - 140)\alpha_8 = 0. \tag{20}$$

The condition of keeping the solutions within the interval of instability, $0 < |\kappa| < 2$, imposes constraints on α_6 and α_8, i.e., α_6 has to be within the interval $-\frac{1}{12} < \alpha_6 < -\frac{1}{60}$, while α_8 must be within the interval $-\frac{1}{40} < \alpha_8 < -\frac{1}{280}$. In each of these cases, there is only one solution within the instability interval. That is, the frequencies of zero growth rate are given by

$$\kappa = \pm\sqrt{5 + \frac{\sqrt{-\alpha_6\,(1 + 10\alpha_6)}}{\sqrt{2}\alpha_6}}$$

for the evolution equation of the 6*th* order and

$$\kappa = \pm\frac{1}{\sqrt{6}}\left[\sqrt{28 + \frac{\sqrt[3]{2}\sqrt[3]{p}}{\alpha_8} - \frac{28\ 2^{2/3}\alpha_8}{\sqrt[3]{p}}}\right]$$

for the evolution equation of the 8th order, where

$$p = \alpha_8^2\,(27 + 896\alpha_8) + 3\sqrt{3}\sqrt{\alpha_8^4\,[27 + 896\alpha_8\,(2 + 35\alpha_8)]}.$$

Figure 6 shows the modulation frequency κ that gives zero growth rate as a function of the higher-order even operator coefficient, α_4, α_6, or α_8. The solid blue curve is for α_4. This solution exists in the range $-\frac{1}{4} < \alpha_4 < -\frac{1}{12}$. The dark orange dotted-dashed curve is for α_6. This solution exists within the range $-\frac{1}{12} < \alpha_6 < -\frac{1}{60}$. Finally, the yellow dashed curve is for α_8. This solution exists within the range $-\frac{1}{40} < \alpha_8 < -\frac{1}{280}$. As we can expect, the changes induced by higher-order terms occur at smaller values of the corresponding coefficients. Otherwise, there are no significant changes in the MI dynamics with the increasing order of the equation being considered.

VIII. CONCLUSIONS

Although the basic NLSE in its simplest form describes the main features of MI, its applicability cannot be extended to more complex systems, such as ultra-short pulse propagation in highly nonlinear optical fibers and deep water wave dynamics, where higher-order effects become more important.

In this work, we have studied the influence of the higher-order terms in the extended NLSE on the dynamics of modulation instability and ABs. Using the 4th order equation as an example, we have investigated changes in the growth rate of instability and the evolution of breathers in space-time and frequency domains. We have presented the trajectories that correspond to the full growth-decay modulation cycle of the breather. In particular, we have found that the spectral content of the AB can be efficiently controlled by the coefficients of higher-order terms. Also, energy transfer into side-bands is increased at certain values of these coefficients.

One of the differences from the NLSE case is the splitting of the instability band into two sub-bands, with zero growth rate at a point between them. This point of zero growth rate is found for the 4th, 6th, and 8th order extensions of the NLSE. The AB is transformed into a stationary periodic solution at this point. Characteristics of the ABs, such as the growth rate, maximal amplitude, spectral content, and total phase shift induced by the breather, are different in each of the sub-bands of the instability interval.

ACKNOWLEDGMENTS

N.A. and A.A. acknowledge the support of the Australian Research Council (Discovery Project Nos. DP140100265 and DP150102057).

[1]N. Akhmediev and A. Ankiewicz, *Solitons: Nonlinear Pulses and Beams* (Chapman & Hall, London, 1997).
[2]V. I. Bespalov and V. I. Talanov, "Filamentary structure of light beams in nonlinear liquids," ZhETF Pisma Redaktsiiu **3**, 471 (1966).
[3]T. B. Benjamin and J. E. Feir, "The disintegration of wave trains on deep water part 1. Theory," J. Fluid Mech. **27**, 417–430 (1967).
[4]A. Chabchoub, B. Kibler, J. M. Dudley, and N. Akhmediev, "Hydrodynamics of periodic breathers," Philos. Trans. R. Soc. A **372**, 20140005 (2014).

[5]V. E. Zakharov, "Collapse of Langmuir waves," Sov. Phys. JETP **35**, 908–914 (1972).
[6]A. M. Turing, "The chemical basis of morphogenesis," Philos. Trans. R. Soc. Lond. B **237**, 37–72 (1952).
[7]K. Tai, A. Hasegawa, and A. Tomita, "Observation of modulational instability in optical fibers," Phys. Rev. Lett. **56**, 135 (1986).
[8]E. J. Greer, D. M. Patrick, P. G. J. Wigley, and J. R. Taylor, "Generation of 2 THz repetition rate pulse trains through induced modulational instability," Electron. Lett. **25**, 1246–1248 (1989).
[9]G. P. Agrawal, "Modulation instability induced by cross-phase modulation," Phys. Rev. Lett. **59**, 880 (1987).
[10]A. Demircan and U. Bandelow, "Supercontinuum generation by the modulation instability," Opt. Commun. **244**, 181–185 (2005).
[11]J. C. Travers, A. B. Rulkov, B. A. Cumberland, S. V. Popov, and J. R. Taylor, "Visible supercontinuum generation in photonic crystal fibers with a 400 W continuous wave fiber laser," Opt. Express **16**, 14435–14447 (2008).
[12]J. M. Dudley, G. Genty, F. Dias, B. Kibler, and N. Akhmediev, "Modulation instability, Akhmediev Breathers and continuous wave supercontinuum generation," Opt. Express **17**, 21497–21508 (2009).
[13]D. R. Solli, C. Ropers, P. Koonath, and B. Jalali, "Optical rogue waves," Nature **450**, 1054 (2007).
[14]E. Fermi, J. Pasta, and S. Ulam, "Los Alamos report no. la-1940, 1955," in *Collected Papers of Enrico Fermi*, (University of Chicago Press, 1965), Vol. 2, pp. 977–978.
[15]S. A. Chin, O. A. Ashour, and B. M. R., "Anatomy of the Akhmediev breather: Cascading instability, first formation time, and Fermi-Pasta-Ulam recurrence," Phys. Rev. E **92**, 063202 (2015).
[16]N. Devine, A. Ankiewicz, G. Genty, J. M. Dudley, and N. Akhmediev, "Recurrence phase shift in Fermi–Pasta–Ulam nonlinear dynamics," Phys. Lett. A **375**, 4158–4161 (2011).
[17]G. VanSimaeys, P. Emplit, and M. Haelterman, "Experimental demonstration of the Fermi-Pasta-Ulam recurrence in a modulationally unstable optical wave," Phys. Rev. Lett. **87**, 033902 (2001).
[18]N. Akhmediev and A. Ankiewicz, "Modulation instability, Fermi-Pasta-Ulam recurrence, rogue waves, nonlinear phase shift, and exact solutions of the Ablowitz-Ladik equation," Phys. Rev E **83**, 046603 (2011).
[19]G. P. Agrawal, *Nonlinear Fiber Optics*, 5th ed. (Academic Press, 2012).
[20]V. E. Zakharov and A. B. Shabat, "Exact theory of two-dimensional self-focusing and one-dimensional self-modulation of waves in nonlinear media," J. Exp. Theor. Phys. **34** 62–69 (1972).
[21]N. Akhmediev and V. I. Korneev, "Modulation instability and periodic solutions of the nonlinear Schrödinger equation," Theor. Math. Phys. **69**, 1089–1093 (1986).
[22]N. Akhmediev, V. Eleonsky, and N. Kulagin, "Generation of periodic trains of picosecond pulses in an optical fiber: Exact solutions," Sov. Phys. JETP **62**, 894–899 (1985).
[23]A. Chowdury, "Solitons, breathers and rogue waves in nonlinear media," Ph.D. thesis, see https://openresearch-repository.anu.edu.au/handle/1885/104531.
[24]F. Baronio, "Akhmediev breathers and Peregrine solitary waves in a quadratic medium," Opt. Lett. **42**, 1756 (2017).
[25]C. Mahnke and F. Mitschke, "Possibility of an Akhmediev breather decaying into solitons," Phys. Rev. A **85**, 033808 (2012).
[26]B. Frisquet, B. Kibler, and G. Millot, "Collision of Akhmediev breathers in nonlinear fiber optics," Phys. Rev. X **3**, 041032 (2013).
[27]M. Erkintalo, G. Genty, B. Wetzel, and J. M. Dudley, "Akhmediev breather evolution in optical fiber for realistic initial conditions," Phys. Lett. A **375**, 2029–2034 (2011).
[28]D. D. Eeltink, A. Lemoine, H. Branger, O. Kimmoun, C. Kharif, J. D. Carter, M. Chabchoub, A. Brunetti, and J. Kasparian, "Spectral up- and downshifting of Akhmediev breathers under wind forcing," Phys. Fluids **29**, 107103 (2017).
[29]N. V. Priya, M. Senthilvelan, and M. Lakshmanan, "Akhmediev breathers, Ma solitons, and general breathers from rogue waves: A case study in the Manakov system," Phys. Rev. E **88**, 022918 (2013).
[30]S. A. El-Tantawy and E. I. El-Awady, "Cylindrical and spherical Akhmediev breather and freak waves in ultracold neutral plasmas," Phys. Plasmas **25**, 012121 (2018).
[31]G. P. Agrawal, "Nonlinear fiber optics: Its history and recent progress [invited]," J. Opt. Soc. Am. B **28**, A1–A10 (2011).
[32]E. J. Kelleher, J. C. Travers, S. V. Popov, and J. R. Taylor, "Role of pump coherence in the evolution of continuous-wave supercontinuum generation initiated by modulation instability," J. Opt. Soc. Am. B **29**, 502–512 (2012).
[33]V. E. Zakharov, "Stability of periodic waves of finite amplitude on the surface of a deep fluid," J. Appl. Mech. Tech. Phys. **9**, 190–194 (1968).
[34]H. C. Yuen and B. M. Lake, "Instabilities of waves on deep water," Ann. Rev. Fluid Mech. **12**, 303–334 (1980).
[35]A. Chabchoub, N. Hoffmann, M. Onorato, G. Genty, J. M. Dudley, and N. Akhmediev, "Hydrodynamic supercontinuum," Phys. Rev. Lett. **111**, 054104 (2013).
[36]K. B. Dysthe, "Note on a modification to the nonlinear Schrödinger equation for application to deep water waves," Proc. R. Soc. Lond. A **369**, 105–114 (1979).
[37]Y. V. Sedletsky, "The fourth-order nonlinear Schrödinger equation for the envelope of stokes waves on the surface of a finite-depth fluid," J. Exp. Theor. Phys. **97**, 180–193 (2003).
[38]A. Slunyaev, "A high-order nonlinear envelope equation for gravity waves in finite-depth water," J. Exp. Theor. Phys. **101**, 926–941 (2005).
[39]T. Kano, "Normal form of nonlinear Schrödinger equation," J. Phys. Soc. Jpn. **58**, 4322–4328 (1989).
[40]D. J. Kedziora, A. Ankiewicz, A. Chowdury, and N. Akhmediev, "Integrable equations of the infinite nonlinear Schrödinger equation hierarchy with time variable coefficients," Chaos **25**, 103114 (2015).
[41]A. Chowdury, D. J. Kedziora, A. Ankiewicz, and N. Akhmediev, "Soliton solutions of an integrable nonlinear Schrödinger equation with quintic terms," Phys. Rev. E **90**, 032922 (2014).
[42]A. Ankiewicz, D. J. Kedziora, A. Chowdury, U. Bandelow, and N. Akhmediev, "Infinite hierarchy of nonlinear Schrödinger equations and their solutions," Phys. Rev. E **93**, 012206 (2016).
[43]A. Chowdury, D. J. Kedziora, A. Ankiewicz, and N. Akhmediev, "Breather-to-soliton conversions described by the quintic equation of the nonlinear Schrödinger hierarchy," Phys. Rev. E **91**, 032928 (2015).
[44]T. B. Benjamin, "Instability of periodic wavetrains in nonlinear dispersive systems," Proc. R. Soc. Lond. A **299**, 59–76 (1967).
[45]V. Zakharov and L. Ostrovsky, "Modulation instability: The beginning," Phys. D: Nonlinear Phenom. **238**, 540–548 (2009).
[46]K. Trulsen, I. Kliakhandler, K. B. Dysthe, and M. G. Velarde, "On weakly nonlinear modulation of waves on deep water," Phys. Fluids **12**, 2432–2437 (2000).
[47]K. Dysthe, H. E. Krogstad, and P. Müller, "Oceanic rogue waves," Annu. Rev. Fluid Mech. **40**, 287–310 (2008).
[48]R. Hirota, "Exact envelope-soliton solutions of a nonlinear wave equation," J. Math. Phys. **14**, 805–809 (1973).
[49]A. Ankiewicz, J. M. Soto-Crespo, and N. Akhmediev, "Rogue waves and rational solutions of the Hirota equation," Phys. Rev. E **81**, 046602 (2010).
[50]K. Porsezian, "Completely integrable nonlinear Schrödinger type equations on moving space curves," Phys. Rev. E **55**, 3785–3788 (1997).
[51]A. Ankiewicz and N. Akhmediev, "Higher-order integrable evolution equation and its soliton solutions," Phys. Lett. A **378**, 358–361 (2014).
[52]A. Ankiewicz, Y. Wang, S. Wabnitz, and N. Akhmediev, "Extended nonlinear Schrödinger equation with higher-order odd and even terms and its rogue wave solutions," Phys. Rev. E **89**, 012907 (2014).
[53]M. Lakshmanan, K. Porsezian, and M. Daniel, "Effect of discreteness on the continuum limit of the Heisenberg spin chain," Phys. Lett. A **133**, 483–488 (1988).
[54]S. M. Hoseini and T. R. Marchant, "Solitary wave interaction and evolution for a higher-order Hirota equation," Wave Motion **44**, 92–106 (2006).
[55]A. Chowdury, A. Ankiewicz, and N. Akhmediev, "Moving breathers and breather-to-soliton conversions for the Hirota equation," Proc. R. Soc. A **471**, 20150130 (2015).
[56]A. Chowdury and W. Krolikowski, "Breather-to-soliton transformation rules in the hierarchy of nonlinear schrödinger equations," Phys. Rev. E **95**, 062226 (2017).
[57]A. Chowdury, W. Krolikowski, and N. Akhmediev, "Breather solutions of a fourth-order nonlinear Schrödinger equation in the degenerate, soliton, and rogue wave limits," Phys. Rev. E **96**, 042209 (2017).
[58]K. Porsezian, M. Daniel, and M. Lakshmanan, "On the integrability aspects of the one-dimensional classical continuum isotropic biquadratic Heisenberg spin chain," J. Math. Phys. **33**, 1807–1816 (1992).
[59]L. H. Wang, K. Porsezian, and J. S. He, "Breather and rogue wave solutions of a generalized nonlinear Schrödinger equation," Phys. Rev. E **87**, 053202 (2013).
[60]N. Akhmediev, A. Ankiewicz, J. M. Soto-Crespo, and J. M. Dudley, "Universal triangular spectra in parametrically-driven systems," Phys. Lett. A **375**, 775–779 (2011).